2D lattice model for fracture in brittle materials

Jan Kozicki and Jacek Tejchman
Faculty of Civil and Environmental Engineering, Gdansk University of Technology
Narutowicza 11/12, 80-952 Gdansk-Wrzeszcz
e-mail: tejchmk@pg.gda.pl

Abstract

The numerical simulations show the potential of a lattice discrete approach to model fracture in brittle materials during different two-dimensional quasi-static processes of loading behaviour. The 2D calculations were carried out for brittle specimens subject to uniaxial compression, uniaxial extension and shear. The effect of the specimen size on the global stress-strain diagram during uniaxial tension was also investigated. The advantages and disadvantages of the model were outlined.

Keywords: beam, brittle material, discrete method, fracture, lattice model, size effect

1. Introduction

Cracks are a fundamental phenomenon in brittle materials (Bazant 2003). The fracture process is a major case of damage in brittle materials under mechanical loading caused by a significant degradation of the material strength. It is highly complex due to a heterogeneous structure of brittle materials over many different length scales, e.g. changing in concrete from the few nanometers (hydrated cement) to the milimeters (aggregate particles). A realistic description of the fracture process is of a major importance to ensure safety of the structure and to optimise the material behaviour.

The phenomenon of the propagation of cracks in brittle materials can be modelled with continuous and discontinuous models. Continuum models describing the mechanical behaviour of concrete were formulated within non-linear elasticity (Liu et al. 1977, Palaniswamy and Shah 1974, Kompfner 1983), rate-independent plasticity (Mróz 1972, Pietruszczak et al. 1988, Klisinski and Mróz 1988, Menetrey and Willam 1995, Bobinski and Tejchman 2005a), damage theory (Dragon and Mróz 1979, Peerlings et al.

1998, di Prisco and Mazars 1996, Bobinski and Tejchman 2005b), endochronic theory (Bazant and Bhat 1976, Bazant and Shieh 1978), coupled damage and plasticity (Klisinski and Mróz 1988, de Borst et al. 1999, Ibrahimbegovic et al. 2003), microplane theory (Bazant and Ozbolt 1990). To properly model the thickness and spacing of cracks, continuum models require an extension in the form of a characteristic length. Such extension can by done with strain gradient (Zbib and Aifantis 1989, Mühlhaus and Aifantis 1991, Peerlings et al. 1998, Pamin and de Borst 1998, Chen et al. 2001, Pamin 2004), viscous (Sluys 1992, Sluys and de Borst 1994) and non-local terms (Bazant 1986, Pijaudier-Cabot and Bazant 1987, Bazant and Jirasek 2002, Bobinski and Tejchman 2004). Within discontinuous methods, a discrete element method DEM (Donze at al. 1999, D'Addetta et al. 2003) and a lattice model (Herrmann et al. 1989, Vervuut et al. 1994, van Mier et al. 1995, Schlangen and Garboczi 1997, Lilliu and van Mier 2003, Vidya Sagar 2004) were applied among others. The lattice models are the simplest discrete models to simulate fracture in brittle materials consisting of a main crack with various branches, secondary cracks and microcracks.

The intention of our research is to describe the mechanism of fracture in quasi-brittle materials using continuum (Bobinski and Tejchman 2004, 2005a, 2005b) and discrete models (Kozicki and Tejchman 2003). In the case of discrete models, a lattice approach was used in the first step. The goal of simulations presented in this paper was to present the potential of a lattice model to model the fracture process in brittle materials during different two-dimensional processes of loading (uniaxial compression and extension, and shear). In contrast to a lattice model presented by Vervuut et al. (1994), van Mier et al. (1995), Schlangen and Garboczi (1997), and Lilliu and van Mier (2003), a geometric type lattice model was used. Owing to that, the computational effort was significantly reduced.

2. Lattice model

In a conventional lattice model used to describe the fracture process in concrete or reinforced concrete (Vervuut et al. 1994, van Mier et al. 1995, Schlangen and Garboczi 1997, Lilliu and van Mier 2003), each quasi-brittle material is discretized as a lattice composed of Bernoulli beams (Fig.1) that transfer normal forces, shear forces and bending moments. Fracture is simulated by performing a linear elastic analysis under loading and removing a beam element that exceeds tensile strength. Normal forces, shear forces and moments are calculated using a conventional simple beam theory. The stiffness matrix is constructed for the entire lattice. The displacement vector is calculated similarly as in the conventional FEM (by multiplication of the inverse global stiffness matrix with the load vector). The heterogeneity of the

material is taken into account by assigning different strengths to beams (using a Gaussian or Weibull distribution) or by assuming random dimensions of beams and random geometry of the lattice mesh or by a mapping of different material properties to beams corresponding to the cement matrix, aggregate and interface zones (Fig.2), respectively in the case of concrete. To obtain aggregate overlay in the lattice, a Fuller curve is usually chosen for the distribution of grains. The ratio between the beam height and the beam length determines the Poisson's ratio. The beam length in concrete should be smaller than $l_b<d_a^{min}$ (where d_a^{min} is the minimum aggregate diameter). The model can identify micro-cracking, crack branching, crack tortuosity and bridging which lead to the fracture process to be followed until complete failure (Vidya Sagar 2004). It enables also to capture a size effect during tension (Vidya Sagar 2004). The advantages of this approach are simplicity and a direct insight in the fracture process on the level of the micro-structure. A complex crack patterning can be reproduced. Therein a limited number of parameters is needed. By applying an elastic-purely brittle local fracture law at the particle level, global softening behaviour is observed. The disadvantages of the classical lattice model are following: the results depend on the beam size and direction of loading, the response of the material is too brittle (due to the assumed brittleness of single beams), the compressed beam elements overlap each other and an extreme computational effort on the structure level is needed. The first disadvantage can be removed by assuming a heterogeneous structure (Schlangen and Garboczi 1997). In turn, the second drawback can be improved by 3D calculations and consideration of very small particles (Lilliu and van Mier 2003), and by applying a non-local approach in calculations of beam deformations (Schlangen and Garboczi 1997).

In our 2D-lattice model, the quasi-brittle material was discretized in the form of a triangular grid including beam elements. The distribution of beams was assumed to be completely random analogously to a Voronoi's scheme. First, a triangular grid was created in the material with the side dimensions equal to g (Fig.3). In each triangles of the grid, additional interior squares were assumed with an area of $s\times s$ ($s<g$). Next, one point was selected at random within these interior squares. Later, all points inside of squares were connected with neighbouring ones within a distance of r_{max} to create a non-uniform mesh of beams, where the maximum beam length was r_{max} (e.g. $r_{max}=2g$), the minimum beam length was r_{min} (e.g. $r_{min}=0.1g$ for $s=0.6g$) and the minimum angle between beams was assumed to be as α (e.g. $\alpha=20^o$). An uniform triangular mesh could be obtained only for the parameter $s=0$. Using this grid generation method, the beams could cross each other in two dimensional calculations (similarly as in the lattice model by Burt and Dougill (1977)) but they did not intersect each other in three-dimensional analyses. The beams possessed a longitudinal stiffness described by the parameter k_l (which controls the changes of the beam

length) and a bending stiffness described by the parameter k_b (which controls the changes of the angle between beams).

In contrast to a conventional lattice method (Schlangen and Garboczi 1997), our model is of a kinematic type, i.e. the calculations of beam displacements were carried out on the basis of the consideration of successive geometry changes of beams due to translation, rotation and deformation (normal and bending). Thus, the global stiffness matrix was not built and the calculation method had an explicit character. The displacement of the center of each beam was calculated as the average displacement of two end nodes belonging to the beam from the previous iteration step:

$$\Delta\vec{X}_i = \frac{\Delta\vec{X}_i^{\,A} + \Delta\vec{X}_i^{\,B}}{2}, \tag{1}$$

wherein $\Delta\vec{X}_i^{\,A}$ and $\Delta\vec{X}_i^{\,B}$ – displacement of the end nodes '*A*' and '*B* 'in the beam '*i*', respectively. The displacement vector of each beam node was calculated by averaging the displacements of the end of beams belonging to this node caused by translation, rotation, normal and bending deformations (Fig.4):

$$\Delta\vec{X}^{\,j} = \frac{1}{n}[\sum_i \left(\vec{W}_i^{\,j} + \vec{R}_i^{\,j}\right)] + \sum_i [\frac{k_{li}^{\,j}\vec{D}_i^{\,j} + k_{bi}^{\,j}\vec{B}_i^{\,j}}{k_{li}^{\,j} + k_{bi}^{\,j}}], \tag{2}$$

wherein $\Delta\vec{X}^{\,j}$ - resultant node displacement, $\vec{W}$ - node displacement due to the beam translation, $\vec{R}$ - node displacement due to the beam rotation, k_l - longitudinal stiffness k_b - bending stiffness, $\vec{D}$ - node displacement due to a change of the beam length (induced by the longitudinal stiffness parameter k_l), $\vec{B}$ - node displacement due to a change of the rotation angle between beams (induced by the bending stiffness parameter k_b), *i* - beam number, *j* - node number and *n* – number of beams belonging to the same node. The node displacements are calculated successively during each calculation step. ~~loading increment.~~

The calculation method of the resultant node displacement vector by Eq.2 is shown below on the example of a simple lattice composed of 4 beams during one displacement increment (Fig.5). The co-ordinates of the nodes '*1-5*'are following: node '*1*' (0.4, 1.5), node '*2*' (0.8, 0.6), node '*3*' (0.0, 0.0), node '*4*' (1.6, 0.5) and node '*5*' (2.0, 0.0). The nodes '*3*' and '*5*' are fixed and the node '*1*' is assumed to displace to the point with the new co-ordinates (0.58, 1.42). The displacement vectors of the node '*2*' in the beams '*1*',

'*2*' and '*3*' are: $\vec{W}_1^2=(0.09,-0.04)$, $\vec{W}_2^2=(0,0)$, $\vec{W}_3^2=(0,0)$, $\vec{R}_1^2=(-0.065,-0.012)$, $\vec{R}_2^2=(0,0)$, $\vec{R}_3^2=(0,0)$, $\vec{D}_1^2=(0.035,-0.131)$, $\vec{D}_2^2=(0,0)$, $\vec{D}_3^2=(0,0)$, $\vec{B}_1^2=(0.124,0.044)$, $\vec{B}_2^2=(0.44,-0.064)$ and $\vec{B}_3^2=(-0.006,0.041)$, respectively (with the rotation angle of the node '*2*': $\Delta\varphi_1^2=-8.9^o$ (beam '*1*'), $\Delta\varphi_1^2=4.45^o$ (beam '*2*'), and $\Delta\varphi_1^2=-2.97^o$ (beam '*3*')). For the stiffness parameters k_b=0.6 and k_l=1.0, the resultant displacement vector of the node '*2*' is equal to (Eq.2):

$$\Delta\vec{X}^2=\frac{1}{3}\left(\vec{W}_1^2+\vec{W}_2^2+\vec{W}_3^2+\vec{R}_1^2+\vec{R}_2^2+\vec{R}_3^2\right)+\left(\frac{k_{l1}^2\vec{D}_1^2+k_{l2}^2\vec{D}_2^2+k_{l3}^2\vec{D}_3^2+k_{b1}^2\vec{B}_1^2+k_{b2}^2\vec{B}_2^2+k_{b3}^2\vec{B}_3^2}{k_{l1}^2+k_{l2}^2+k_{l3}^2+k_{b1}^2+k_{b2}^2+k_{b3}^2}\right)=$$

$$=\frac{1}{3}[(0.09,-0.04)+(0,0)+(0,0)+(-0.065,-0.012)+(0,0)+(0,0)]+$$

$$\left(\frac{[(0.035,-0.131)+(0.0)+(0,0)]\cdot 1.0+[(0.124,0.044)+(0.044,-0.064)+(0.006,0.041)]\cdot 0.6}{(1.0+1.0+1.0+0.6+0.6+0.6)}\right)= \qquad (3)$$

$$=(0.037,-0.042),$$

and the new co-ordinates of the node '2' are (0.837, 0.558). In turn, the displacement vectors of the node '*4*' in the beams '*3*' and '*4*' are: $\vec{W}_3^4=(0,0)$, $\vec{W}_4^4=(0,0)$, $\vec{R}_3^4=(0,0)$, $\vec{R}_4^4=(0,0)$, $\vec{D}_3^4=(0,0)$, $\vec{D}_4^4=(0,0)$, $\vec{B}_3^4=(-0.006,-0.041)$ and $\vec{B}_4^4=(0,0)$, respectively (with the rotation angle of the node '*4*': $\Delta\varphi_3^4=-2.97^o$ (beam '*3*') and $\Delta\varphi_4^4=2.97^o$ (beam '*4*')). The resultant displacement vector of the node '*4*' is equal to (Eq.2):

$$\Delta\vec{X}^4=\frac{1}{2}\left(\vec{W}_3^4+\vec{W}_4^4+\vec{R}_3^4+\vec{R}_4^4\right)+\left(\frac{k_{l3}^4\vec{D}_3^4+k_{l4}^4\vec{D}_4^4+k_{b3}^4\vec{B}_3^4+k_{b4}^4\vec{B}_4^4}{k_{l3}^4+k_{l4}^4+k_{b3}^4+k_{b4}^4}\right)=$$

$$=\frac{1}{2}[(0,0)+(0,0)+(0,0)+(0,0)]+\left(\frac{(0,0)\cdot 1.0+[(-0.006,-0.041)+(0,0)]\cdot 0.6}{(1.0+1.0+0.6+0.6)}\right)=(-0.001,-0.007), \quad (4)$$

and the new co-ordinates of the node '4' are (1.599, 0.493). Next, the forces are determined with the aid of normal strains and a modulus of elasticity. For the stiffness parameter k_b=0 in Eq.2, the beams behave as bars. The beams were removed from the lattice if the local critical tensile strain ε_{min} was exceeded in

each beam. In addition, the beams were removed if both the local critical tensile strain ε_{min} or local critical compressive strain ε_{max} were exceeded in each beam. The assumption of a different ratio between the bending stiffness and longitudinal stiffness $p=k_b/l_l$ allowed us to simulate the different Poisson's ratio ν. During simulations presented in the paper, the same local critical strains were assumed for all beams (ε_{min}=0.02% for tension and ε_{max}=0.2% for compression). The following strain increments were assumed on the basis of initial calculations: 0.000032% (uniaxial compression) and 0.000004% (uniaxial tension and shear). Smaller strain increments only insignificantly influenced the results. All calculations were strain controlled.

The 2D calculations were carried out mainly with a brittle specimen size of 100×100 mm^2 ($b\times h$) composed of 20000 beam elements distributed non-uniformly (α=20^o, s=0.6g, $g\approx$1.5 mm, r_{max}=2g). The maximum beam length was about 3 mm and the minimum about 0.6 mm. The modulus of elasticity of all beams was assumed to be E=20 GPa. The computation time with 20000 beams was about 10 hours using PC 3.6 GHz.

3. Numerical results

Figure 6 presents the change of the Poisson's ratio ν versus the parameter stiffness ratio $p=k_b/k_l$ during uniaxial compression with smooth horizontal edges at the beginning of deformation (the beams were not removed). For the stiffness parameter p=0.6, the Poisson's ratio ν=0.2 was obtained (typical value for concrete). If the stiffness parameter p=0.01, the Poisson's ratio was 0.4, and if the parameter p=0.001, the Poisson's ratio was 0.5. In turn, if the parameter p>1, the Poisson's ratio became negative (with the smallest value ν=-1,0 at p=10000). The behaviour of beams with smaller values of $p=k_b/k_I$ corresponded obviously to that of bars (Kozicki and Tejchman 2003, 2005).

The effect of the stiffness parameter $p=k_b/k_l$ on the evolution of the global stress-strain curve σ-ε (vertical normal stress versus the vertical strain) and crack propagation in a brittle specimen during uniaxial compression with smooth edges is shown in Figs.7-10 ($\sigma=P/b$, $\varepsilon=u_2/h$, P – global vertical force, u_2 – vertical displacement of the top edge). Figures 7 and 8 present the results for the case if only the beams subject to tension were removed at ε_{min}=0.02%.

The strength and ductility increase with increasing stiffness parameter p. The material becomes elastic for $p \geq 0.6$ and brittle for $p < 0.025$ ($\varepsilon = 0.3\%$). In the last case, the vertical strain corresponding to the material strength is about 0.03%. The cracks are predominantly vertical (parallel to the loading direction) if $p \geq 0.3$. In the case of $p < 0.1$, the predominant cracks are more inclined.

Figures 9 and 10 present the results for the case if the beams subject to both tension and compression were removed at $\varepsilon_{min} = 0.02\%$, and $\varepsilon_{max} = 0.2\%$.

The results are similar to those in the previous case for $p < 0.3$. The strength increases with increasing p. The material is brittle for $p \leq 0.01$ and $p \geq 0.3$. For $p < 0.3$ the cracks are inclined. In turn, for $p \geq 0.3$, the main crack becomes horizontal (perpendicular to the loading direction).

The effect of the roughness of both horizontal edges on the fracture process during uniaxial compression is shown in Fig.11 for $p = 0.6$ and $p = 0.01$ (with $\varepsilon_{min} = 0.02\%$). The results with very rough edges (horizontal displacements along both edges were assumed to be zero) indicate the appearance of diagonal intersecting cracks and stiff wedges in the material.

The results for uniaxial tension with a small notch at mid-height of the left side and smooth horizontal edges are demonstrated in Figs.12 and 13 for the case of $\varepsilon_{min} = 0.02\%$. The material behaves in the elastic-purely brittle way for all values of p. The strength increases with increasing p, and the brittleness increases with decreasing p. The overall vertical strain corresponding to the peak stress values is about 0.007-0.009% (thus it is smaller than the local ε_{min}). The crack pattern practically does not depend on the parameter p. The main crack is always initiated at the notch and then propagates almost horizontally through the specimen (Fig.13).

The effect of the grid parameter s (influencing the minimum beam length and grid non-uniformity) on the stress-strain curve is shown for uniaxial tension in Fig.14 (smooth edges, $\alpha = 20^o$, $g \approx 1.5$ mm, $r_{max} = 2g$). The strength and the overall vertical strain corresponding to the peak value increase with decreasing s. For $s = 0 \times g$ (uniform distribution of beams), a horizontal crack occurs.

The obtained crack patterns during uniaxial compression and extension ($\varepsilon_{min} = 0.02\%$ and $p = 0.6$) are qualitatively in agreement with laboratory experiments with concrete (van Mier et al. 1995, Schlangen and Garboczi 1997). However, the calculated response of the material during extension is far too brittle.

The results of the fracture process for simple shearing are shown in Fig.15 for smooth and very rough edges (with ε_{min}=0.02%, p=0.6). The main cracks are created in the direction perpendicular to the principal normal stress. The number and inclination of cracks depend both on the edge roughness and parameter p. The inclination of the main interior crack with respect to the bottom increases with increasing p and wall roughness. In the case of smooth edges, more pronounced cracks are created.

Figure 16 describes the behaviour of the specimen with two notches under shear (with ε_{min}=0.02%). The lower part of the specimen under the both notches was fixed. The horizontal displacement was prescribed to the upper part of the specimen. The main cracks spreading between both notches which occur during the process of deformation are curvilinear (p=0.6) or horizontal (p=0.01). The results with p=0.6 match well with laboratory experiments by Nooru-Mohamed (1992).

The effect of the specimen size during uniaxial tension with one notch at the right side and smooth edges is demonstrated in Fig.17 (with ε_{min}=0.02%, p=0.6). The calculations were performed with 3 different specimens: 50×50 mm^2, 100×100 mm^2 and 200×200 mm^2 using 5000, 20000 and 80000 beam elements, respectively. Similarly as in experiments with concrete specimens (van Mier and van Vliet 2003), the strength increases with decreasing specimen size. The vertical strain corresponding to the strength increases also with decreasing specimen size. The stress fluctuations grow with decreasing specimen size.

4. Conclusions

The lattice model is a simple approach to the fracture behaviour in quasi-brittle materials but very useful in studying and understanding the phenomenon of the crack formation. Owing to it, novel (stronger and better) engineering materials can be developed. By using an elastic-purely brittle local fracture law at the particle level of the material, global softening behaviour is obtained. The lattice simulations yield a significant size effect in nominal strength, i.e. the strength increases with decreasing specimen size and increasing size of micro-structure (expressed by the beam length). The heterogeneous 2D-lattice model used in the paper requires for the brittle material composed of one component only 3-4 material parameters (p, E, ε_{min}, ε_{max},) and 4 grid parameters related to the distribution, quantity and length of beams (g, s, α and r_{max}). The obtained results of crack patterns are qualitatively in agreement with experimental ones for concrete. However, the lattice stress-strain outcomes are too brittle.

The calculations with a lattice model will be continued. First, the simulations will be carried out with a real brittle material as concrete assuming different material parameters for cement matrix, aggregate grains and interfacial zones. In addition, the beam strains will be non-locally (influenced by the neighbouring beam strains) calculated to increase the material ductility (Kozicki and Tejchman 2006). To prevent the overlapping of compressed beams, special boundary elements will be introduced. Next, the model will be extended into 3D. The material parameters (p, E and ε_{min},) will be stochastically distributed using a Gaussian or Weibull distribution. The calculations will also be performed with reinforced concrete elements (Schlangen at al. 1994). The results will be directly compared with laboratory tests to identify the stiffness parameters and critical local strain.

References

1. Bazant, Z. P. and Bhat, P. D. Endochronic theory of inelasticity and failure of concrete, *J. Engng. Mech. Div. ASCE*, 102, 1976, pp. 701-722.

2. Bazant, Z. P. Mechanics of distributed cracking, *Appl. Mech. Rev*., 26, 675-705, 1986.

3. Bazant, Z. P. and Shieh, C. L. Endochronic model for nonlinear triaxial behaviour of concrete, *Nucl. Engng. Des.*, 47, 1978, pp. 305-315.

4. Bazant, Z. and Ozbolt, J. Non-local microplane model for fracture, damage and size effect in structures. *J. Engng. Mech. ASCE*, 116, 2485-2505, 1990.

5. Bazant, Z. P. and Jirasek, M. Nonlocal integral formulations of plasticity and damage: survey of progress. *J. Engng. Mech.* 128, 11, 1119-1149, 2002.

6. Bazant, Z. P. *Scaling of Structural Strength.* Hermes-Penton, London, 2003.

7. Bobinski, J., and Tejchman, J. Numerical simulations of localization of deformation in quasi-brittle materials within non-local softening plasticity, *Computers and Concrete,* Vol. 4, 433-455, 2004.

8. Bobinski, J., Tejchman, J. Modelling of concrete behaviour with a non-local continuum damage approach. *Archives of Hydro-Engineering and Environmental Mechanics*, Polish Academy of Sciences, 1, 52, 2, 85-102, 2005a.

9. Bobinski, J. and Tejchman, J. Modelling of size effects in concrete using elasto-plasticity with non-local softening. *Archives of Civil Engineering*, 2005b (under press).

10. de Borst, R., Pamin, J. and Geers, M. On coupled gradient-dependent plasticity and damage theories with a view to localization analysis. *Eur. J. Mech. A/Solids* 18, 6, 939-962, 1999.

11. Burt, N. J. and Dougill, J. W. Progressive failure in a model heterogeneous medium. *J. Eng. Mech. Div. ASCE*, 103, 365-376, 1977.

12. Chen, J., Yuan, H. and Kalkhof, D. A nonlocal damage model for elastoplastic materials based on gradient plasticity theory. *Report Nr.01-13*, Paul Scherrer Institut, 1-130, 2001.

13. D'Addetta, G. A., Kun, F. and Ramm, E. In the application of a discrete model to the fracture process of cohesive granular materials. *Granular Matter* 4, 77-90, 2002.

14. Donze, F. V., Magnier, S. A., Daudeville, L., Mariotti, C. and Davenne, L., Numerical study of compressive behaviour of concrete at high strain rates, *Journal Engineering Mechanics*, 1154-1163, 1999.

15. Dragon, A. and Mróz, Z., A continuum model for plastic-brittle behaviour of rock and concrete, *Int. Journ. Eng. Science*, 17, 1979.

16. Herrmann, H. J., Hansen, A. and Roux, S., Fracture of disordered elastic lattices in two dimensions, *Physical Rev. B*, 39, pp. 637-647, 1989.

17. Ibrahimbegovic, A., Markovic, D. and Gatuing, F., Constitutive model of coupled damage-plasticity and its finite element implementatation, *Eur. J. Finite Elem.*, 12, 4, pp. 381-405, 2003.

18. Klisinski, M. and Mróz, Z. Description of anelastic deformations and damage for concrete (in polish), *Monography*, 193, Technical University of Poznan 1988.

19. Kozicki, J. and Tejchman, J. 1. Discrete methods to describe the behaviour of quasi-brittle and granular materials. *Electronic Proceedings of 16th Engineering Mechanics Conference ASCE*, University of Washington, Seattle, USA, 16.07-18.07.2003, 1-10, 2003.

20. Kozicki, J. and Tejchman, J. Simulations of fracture in concrete elements using a discrete lattice model. *Proc. Int. Conf. Computer Methods in Mechanics CMM 2005*.

21. Kozicki, J. and Tejchman, J. Modelling of fracture process in brittle materials using a lattice model. *Proc. Int. Conf. Euro-C 2006*, Mayerhofen, 03.2006.

22. Kompfner, T. A. Ein Finites Elementmodell für die geometrisch und physikalisch nichtlineare Be2rechnung von Stahlbetonschalen, *PhD thesis*, Stuttgart University, 1983.

23. Lilliu, G. and van Mier J. G. M., 3D lattice type fracture model for concrete. *Engineering Fracture Mechanics*, 70, 927-941, 2003.

24. Liu, T. C. Y., Nilson, A. H. and Slate, F. O., "Biaxial stress-strain relationships for concrete", *J. Engng. Mech. Div. ASCE*, 103, 1977, pp. 423-439.

25. Menetrey, Ph. and Willam, K. J. Triaxial failure criterion for concrete and its generalization, *ACI Structural Journal*, 311-318, 1995.

26. van Mier, J., Schlangen, E. and Vervuurt, A., Lattice type fracture models for concrete. *Continuum Models for Materials with Microstructure*, H.-B. Mühlhaus, ed., John Wiley & Sons, 1995, pp. 341-377.

27. van Mier, J. G. M. and van Vliet, M. R. A. Influence of microstructure of concrete on size/scale effects in tensile fracture. *Engineering Fracture Mechanics*, 70, 2281-2396, 2003.

28. Mróz, Z. Mathematical models of inelastic concrete behaviour, *University Waterlo Press*, 1972, pp. 47-72.

29. Mühlhaus, H.-B. and Aifantis, E.C. A variational principle for gradient plasticity. *Int. J. Solids Structures*, 28, 845-858, 1991.

30. Nooru-Mohamed M. B. Mixed-mode fracture of concrete, *PhD thesis*, University of Delft, 1992.

31. Palaniswamy, R. and Shah, S. P., "Fracture and stress-strain relationship of concrete under triaxial compression", *J. Struct. Div. ASCE*, 100, 1974, pp. 901-916.

32. Pamin, J. and de Borst, R. Simulation of crack spacing using a reinforced concrete model with an internal length parameter. *Arch. App. Mech*., 68 (9), 613-625, 1998.

33. Pamin, J. Gradient-enhanced continuum models: formulation, discretization and applications, *Habilitation Monography*, Cracow University of Technology, Cracow, 2004.

34. Pamin, J. and de Borst, R. Stiffness degradation in gradient-dependent coupled damage-plasticity. *Arch. Mech.*, 51, 3-4, 419-446, 1999.

35. Peerlings, R.H.J., de Borst. R., Brekelmans, W. A. M. and Geers, M. G. D., Gradient enhanced damage modelling of concrete fracture, *Mech. Cohesion.-Friction. Materials*, 3, pp. 323-342, 1998.

36. Pietruszczak, S., Jiang, J. and Mirza, F. A., An elastoplastic constitutve model for concrete", *Int. J. Solids Structures*, 24, 7, 1988, pp. 705-722.

37. Pijaudier-Cabot, G. and Bazant, Z. P. Nonlocal damage theory. *ASCE J. Eng. Mech.*, 113, 1512-1533, 1987.

38. di Prisco, M. and Mazars, J. Crush-crack - a non-local damage model for concrete. *Mechanics of Cohesive-Frictional Materials*, 1, 321-347, 1996.

39. Schlangen, E. and Garboczi, E. J. Fracture simulations of concrete using lattice models: computational aspects. *Engineering Fracture Mechanics*, 57, 319-332, 1997.

40. Sluys, L. J. Wave propagation, localisation and dispersion in softening solids, *Dissertation*, Delft University of Technology, Delft, 1992.

41. Sluys, L. J. and de Borst, R. Dispersive properties of gradient and rate-dependent media, *Mech. Mater.* 183, 131-149, 1994.

42. Vervuut, A., van Mier, J. G. M. and Schlangen, E., Lattice model for analyzing steel-concrete interactions, *Computer Methods and Advances in Geomechanics (*Siriwardane and Zaman, eds.), Balkema, Rotterdam, 1994, pp. 713-718.

43. Vidya Sagar, R. Size effect in tensile fracture of concrete – a study based on lattice model applied to CT-specimen. CD-ROM *Proc. 21th Intern. Congress on Theoretical and Applied Mechanics* ICTAM04, Warsaw, 1-2, 2004.

44. Zbib, H.M. and Aifantis, C.E. A gradient dependent flow theory of plasticity: application to metal and soil instabilities. *Appl. Mech. Reviews*, 42(11), 295-304, 1989.

LIST OF FIGURES

Figure 10: Effect of the ratio stiffness $p=k_b/k_l$ between the bending stiffness and longitudinal stiffness on the crack pattern during uniaxial compression with smooth edges (beams were removed when ε_{min}=0.02% and ε_{max}=0.2%): a) p=0.3, b) p=0.01, c) p=0.001

Figure 11: Evolution of fracture process during uniaxial compression with very rough edges (beams were removed when ε_{min}=0.02%): a) p=0.6, b) p=0.01

Figure 12: Effect of the ratio stiffness $p=k_b/k_l$ between the bending stiffness to the longitudinal stiffness on the stress-strain curve during uniaxial extension (beams were removed when ε_{min}=0.02%): a) p=0.3, b) p=0.025, c) p=0.001

Figure 13: Crack pattern during uniaxial extension in the notched specimen (beams were removed when ε_{min}=0.02%)

Figure 14: Effect of the grid parameter s on the stress-strain curve and crack pattern during uniaxial extension (p=0.3, α=20^o, r_{max}=2g): a) s=0×g, b) s=0.3×g, c) s=0.6×g (beams were removed when ε_{min}=0.02%)

Figure 15: Effect of the stiffness ratio $p=k_b/k_I$ between the bending stiffness to the longitudinal stiffness on the crack pattern during simple shearing (beams were removed when ε_{min}=0.02%): a) p=0.6 (smooth edges), b) p=0.6 (rough edges), c) p=0.01 (rough edges)

Figure 16: Crack propagation in a specimen with two notches under shear (beams were removed when ε_{min}=0.02%): a) p=0.6, b) p=0.01

Figure 17: Effect of specimen size for p=0.01 (beams were removed when ε_{min}=0.02%): A) stress-strain curve for the specimen of 50×50 mm^2 (a), 100×100 mm^2 (b) and 200×200 mm^2(c), B) crack propagation in large (2000×200 mm^2) and small specimen (50×50 mm^2)

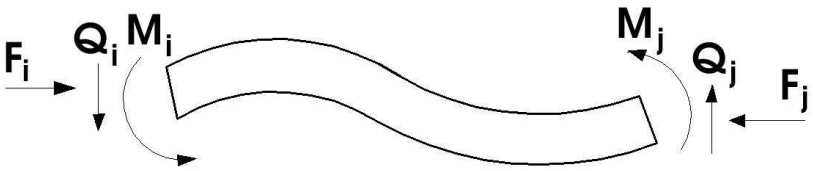

FIGURE 1

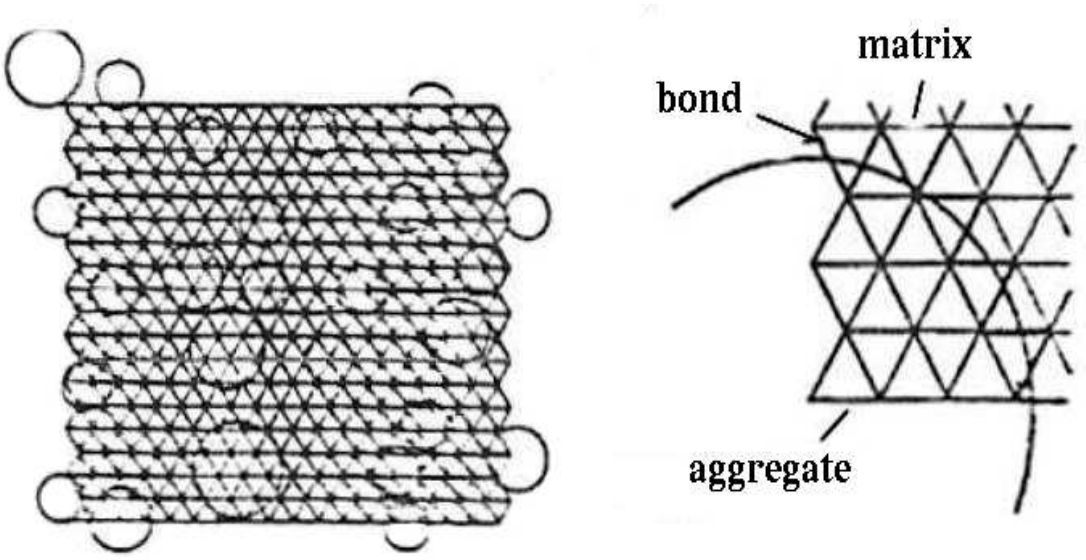

FIGURE 2

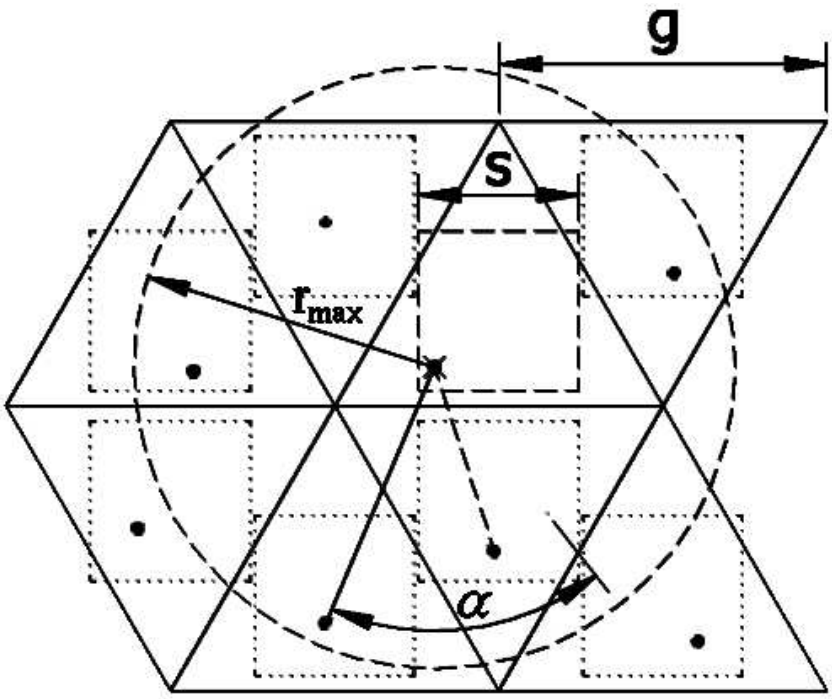

FIGURE 3

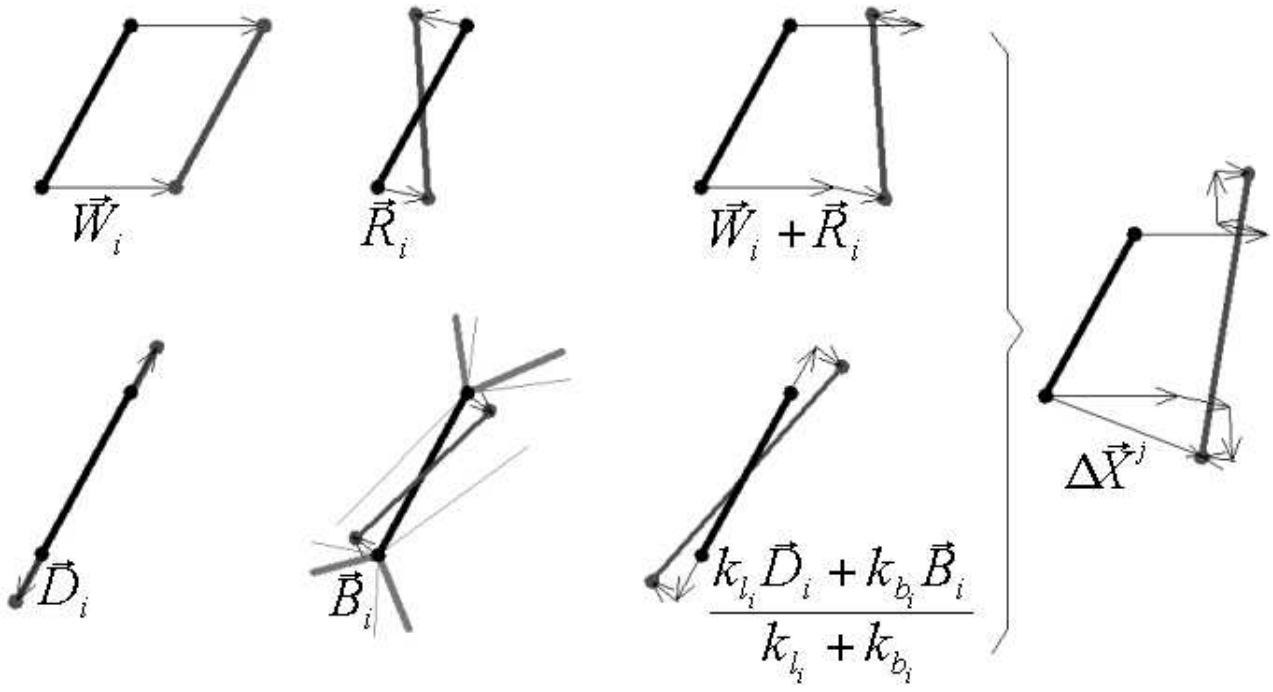
$\vec{W}_i$
$\vec{R}_i$
$\vec{W}_i + \vec{R}_i$
$\vec{D}_i$
$\vec{B}_i$
$\frac{k_{l_i}\vec{D}_i + k_{b_i}\vec{B}_i}{k_{l_i} + k_{b_i}}$
$\Delta\vec{X}^j$

FIGURE 4

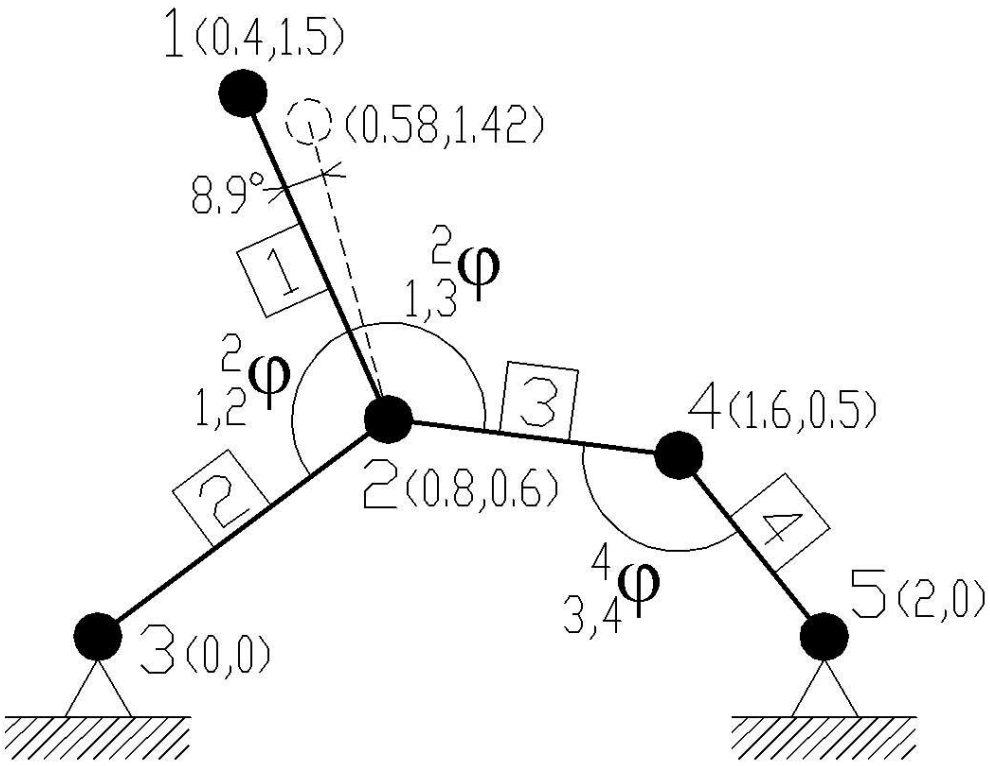

FIGURE 5

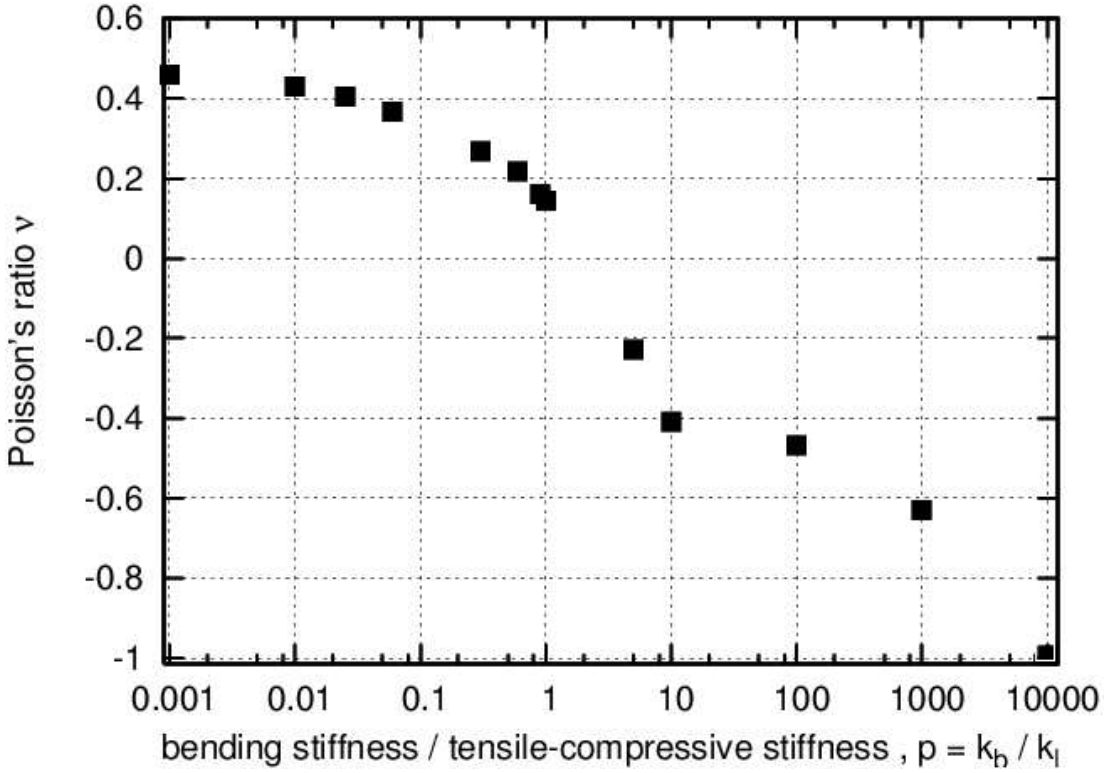
0.6
0.4
0.2
0
-0.2
-0.4
-0.6
-0.8
-1
Poisson's ratio ν
0.001
0.01
0.1
1
10
100
1000
10000
bending stiffness / tensile-compressive stiffness , p = k_b / k_l

FIGURE 6

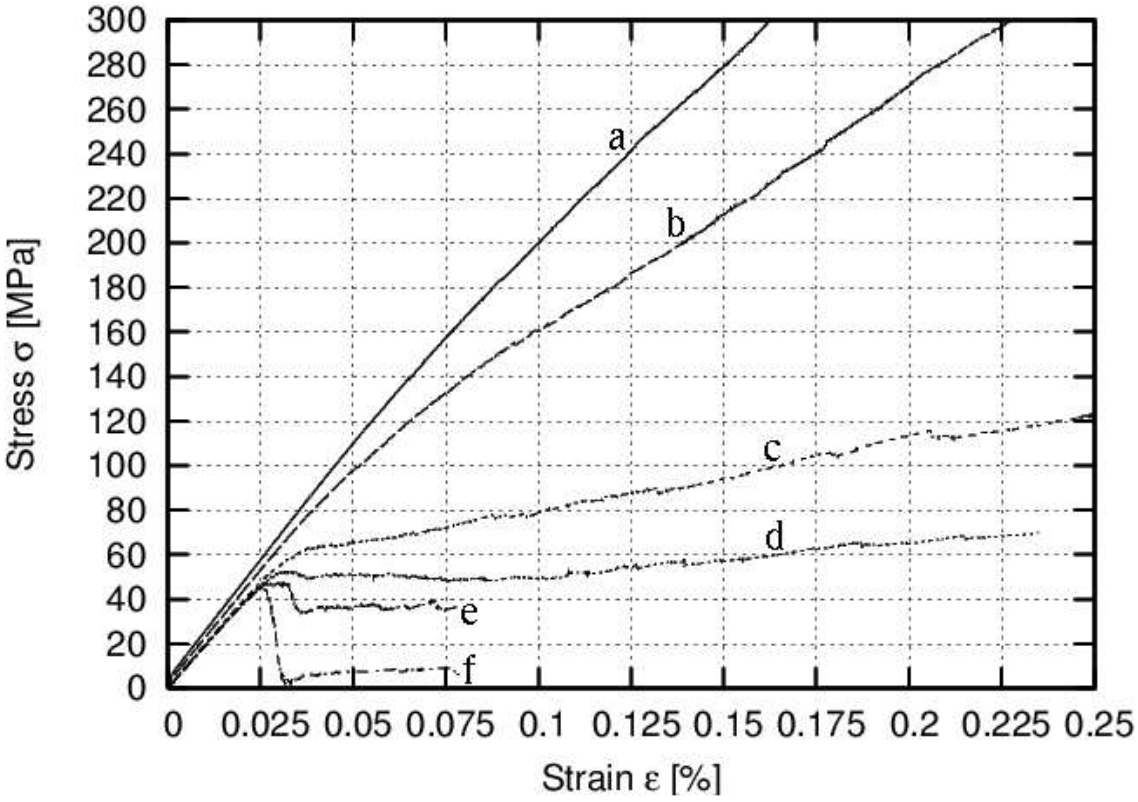
Stress σ [MPa]
Strain ε [%]
300
280
260
240
220
200
180
160
140
120
100
80
60
40
20
0
0
0.025
0.05
0.075
0.1
0.125
0.15
0.175
0.2
0.225
0.25
a
b
c
d
e
f

FIGURE 7

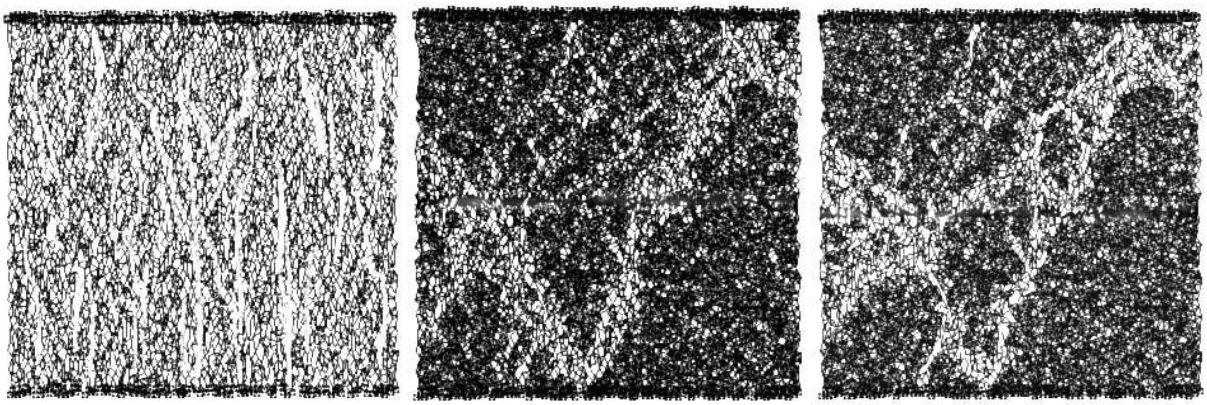

a) b) c)

FIGURE 8

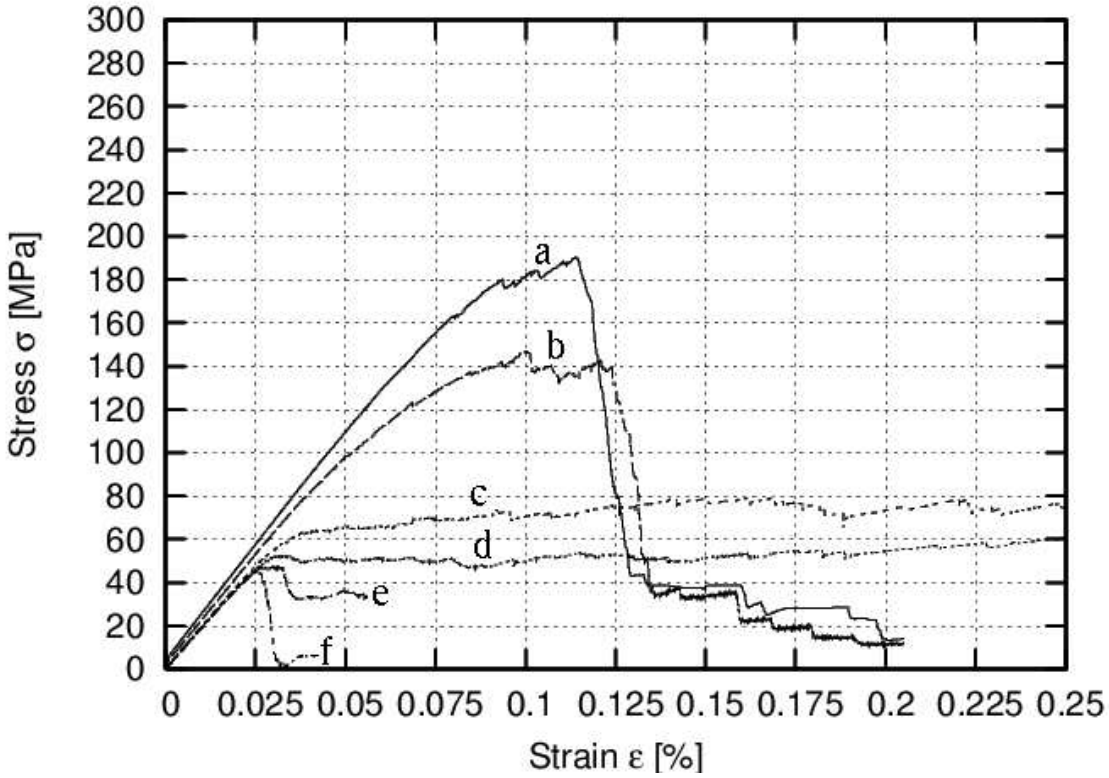
Stress σ [MPa]
Strain ε [%]
300
280
260
240
220
200
180
160
140
120
100
80
60
40
20
0
0
0.025
0.05
0.075
0.1
0.125
0.15
0.175
0.2
0.225
0.25
a
b
c
d
e
f

FIGURE 9

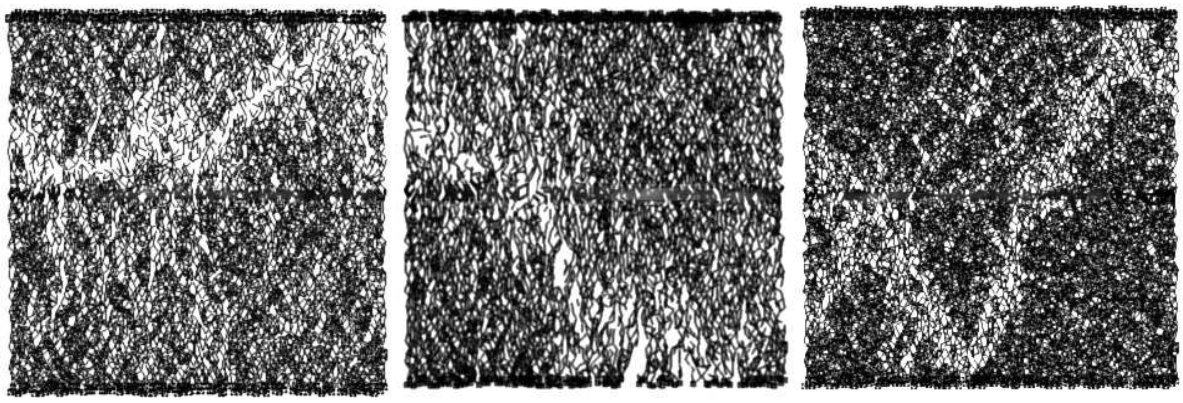

a) b) c)

FIGURE 10

a)

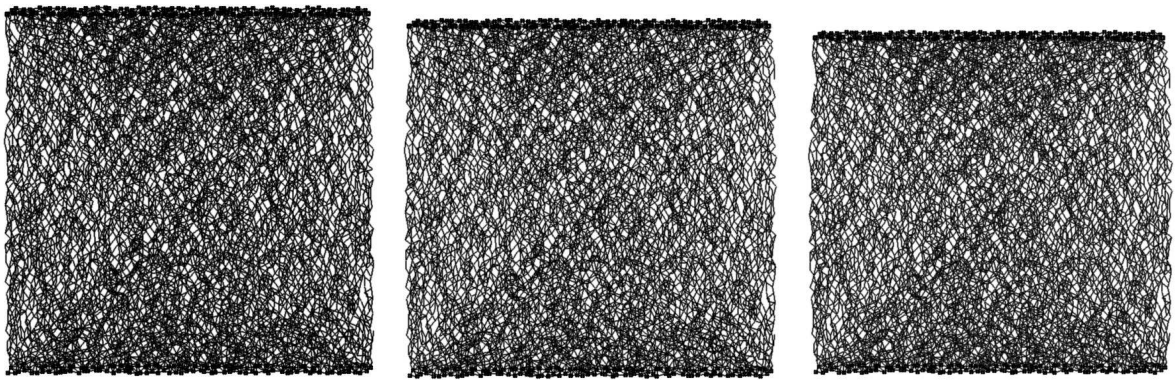

b)

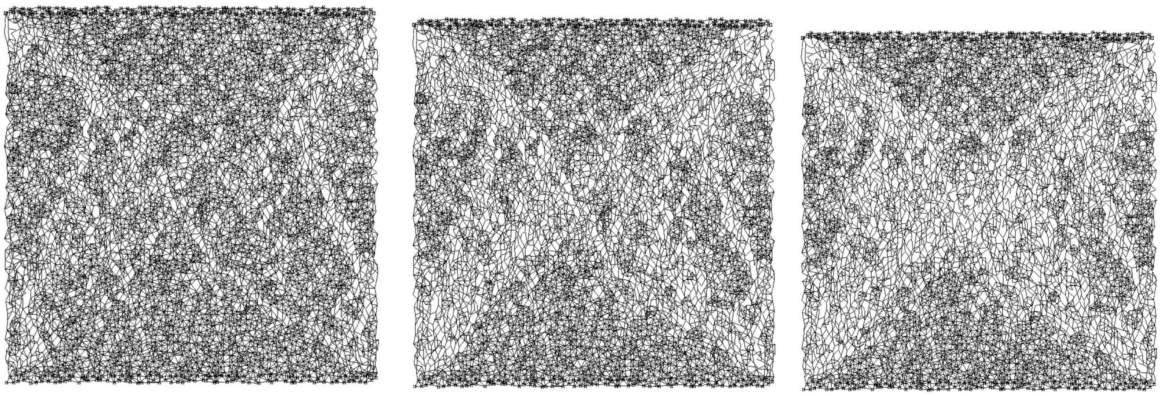

FIGURE 11

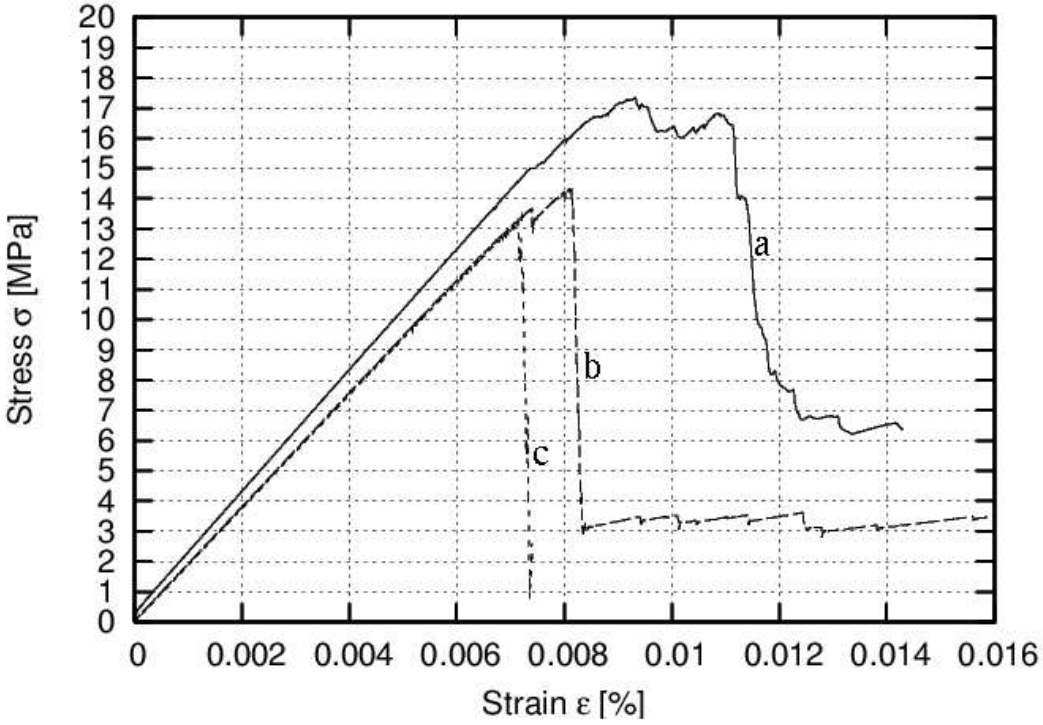
Stress σ [MPa]
Strain ε [%]
a
b
c
0
0.002
0.004
0.006
0.008
0.01
0.012
0.014
0.016

FIGURE 12

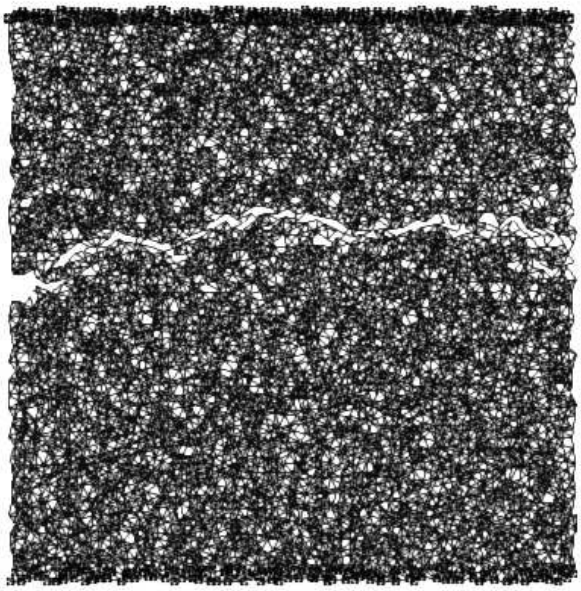

FIGURE 13

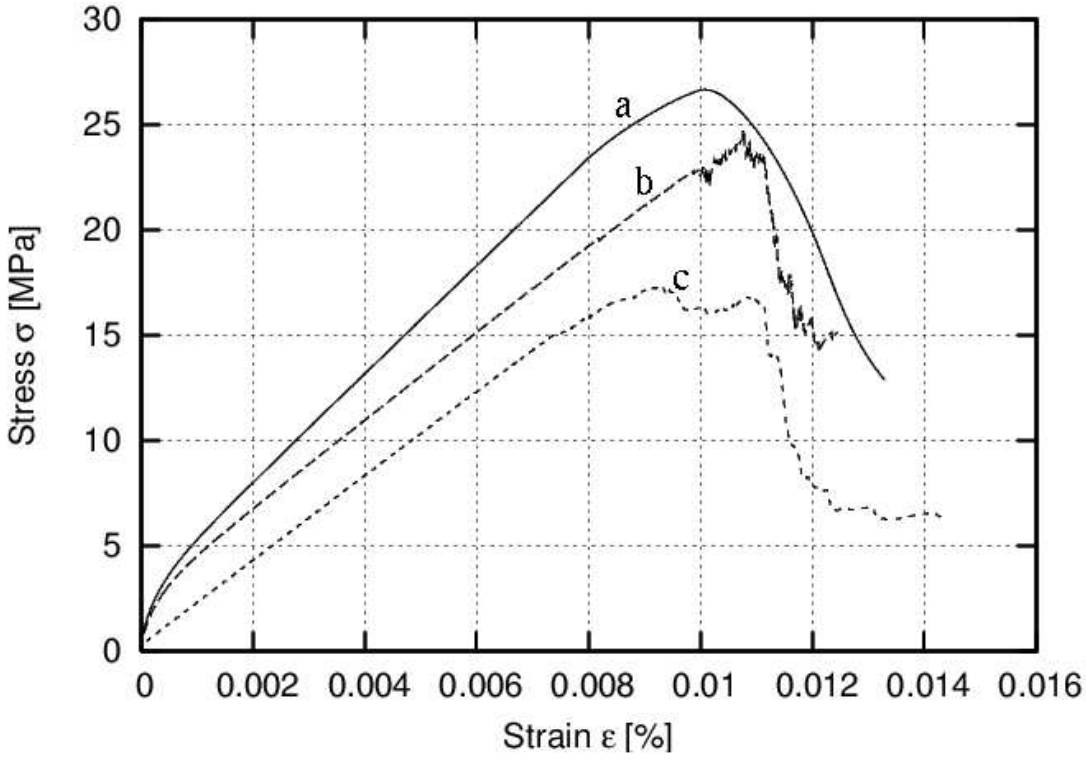

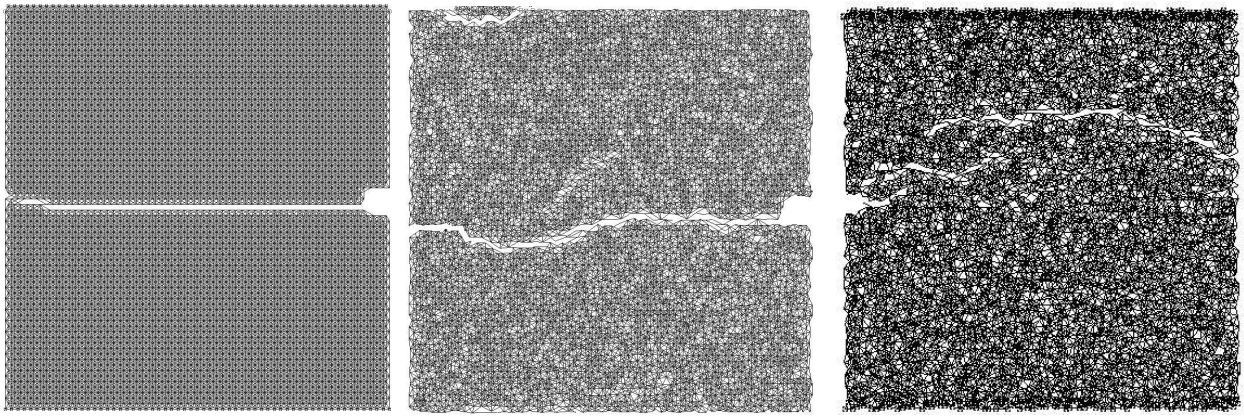

a) b) c)

FIGURE 14

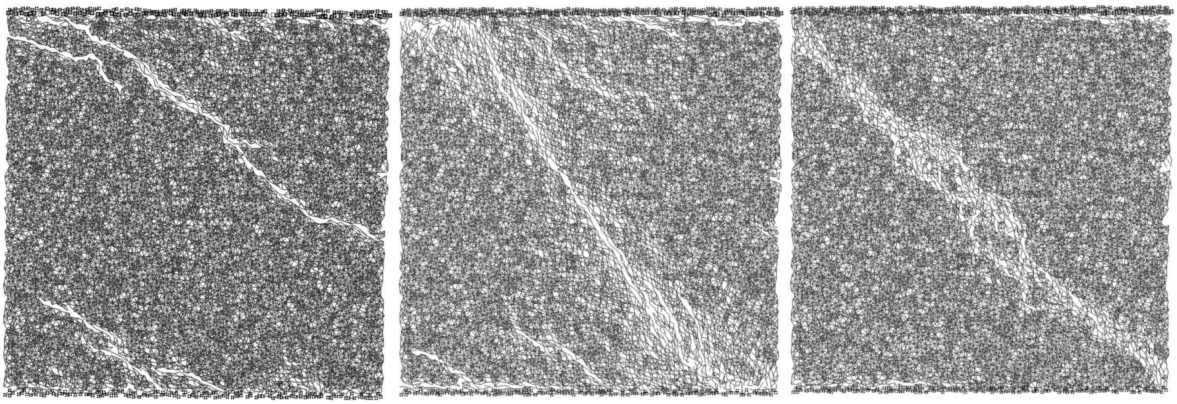

a) b) c)

FIGURE 15

a)

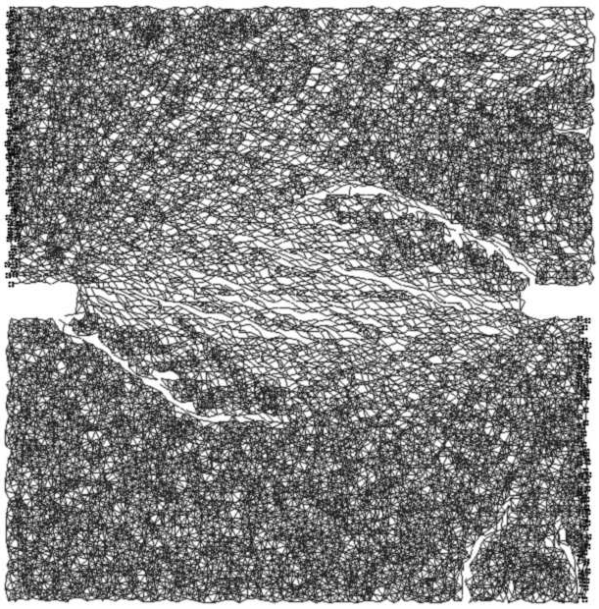

b)

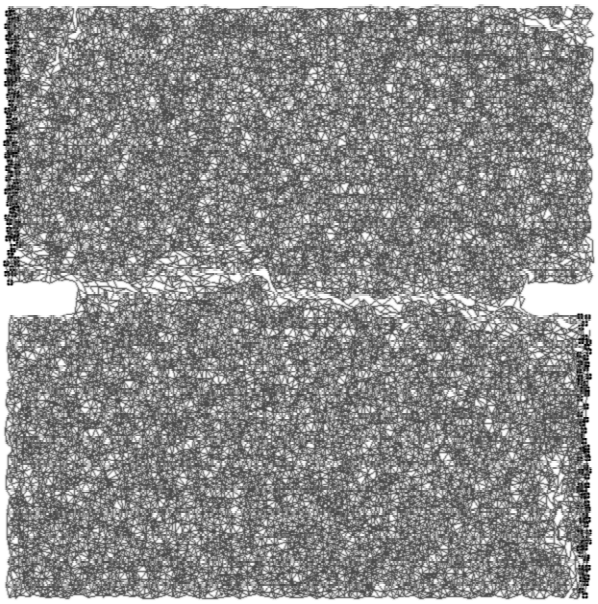

FIGURE 16

A)

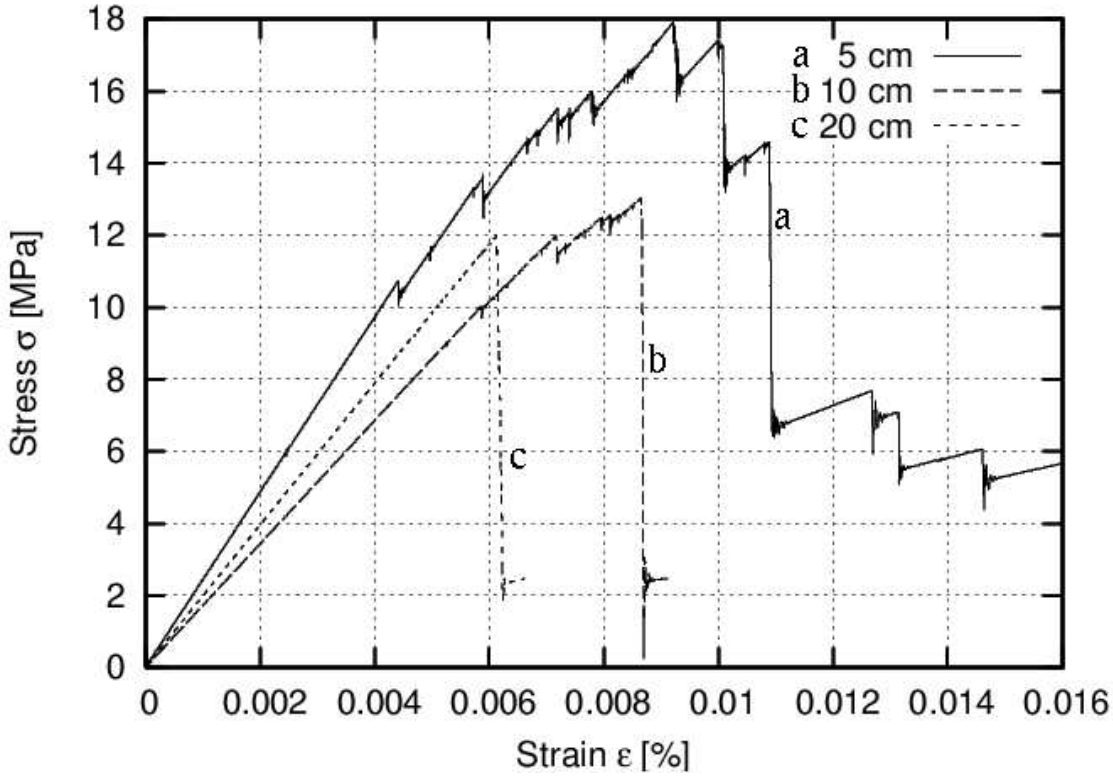
Stress σ [MPa]
Strain ε [%]
a 5 cm
b 10 cm
c 20 cm
a
b
c
0
2
4
6
8
10
12
14
16
18
0
0.002
0.004
0.006
0.008
0.01
0.012
0.014
0.016

B)

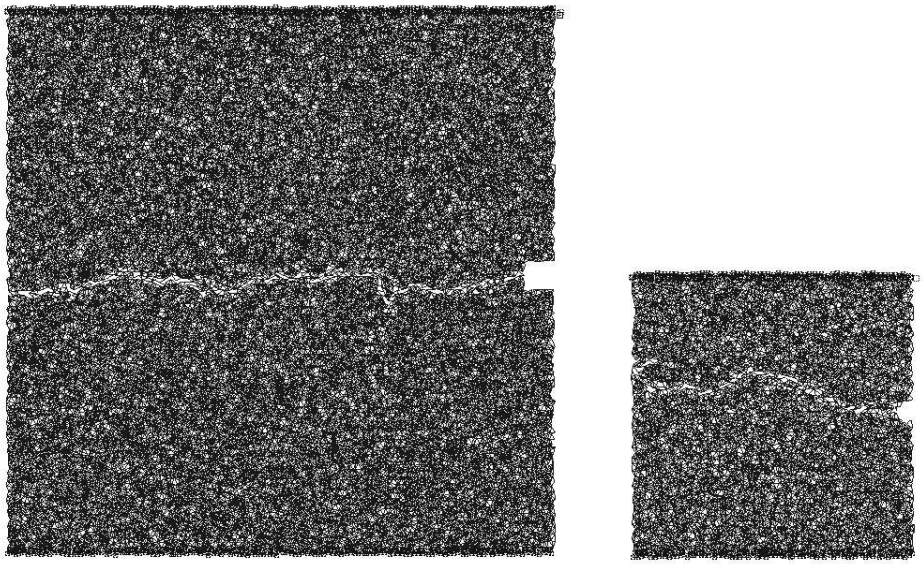

FIGURE 17